



Article

# Influence of Longitudinal and Lateral Forces on the Emission of Tire–Road Particulate Matter and Its Size Distribution

Stefan Schläfle \* , Hans-Joachim Unrau and Frank Gauterin

Institute of Vehicle System Technology, Karlsruhe Institute of Technology, 76131 Karlsruhe, Germany

\* Correspondence: stefan.schlaefle@kit.edu; Tel.: +49-721-608-45328

**Abstract:** The objective of this study was to experimentally determine the mathematical correlations between the loading of the tire, being longitudinal and lateral forces, and the emission of particulate matter (PM) from the tire–road contact. Existing emission factors (EF, emission per vehicle and distance traveled) are the result of long-term measurements, which means that no conclusion can be drawn about the exact driving condition. To determine meaningful emission factors, extensive driving tests were conducted on an internal drum test bench while measuring PM emissions from the tire–road contact in real-time. This showed that the increases in emission over longitudinal and lateral forces can be approximated with fourth-order functions, with lateral forces leading to significantly higher emissions than longitudinal forces for the summer tire investigated. Using the emission functions obtained, a three-dimensional map was created that assigns an EF to each load condition consisting of different longitudinal and lateral forces for one vertical load. With known driving data, the map can be used for future simulation models to predict the total emission of real driving cycles. Furthermore, the results show that the average particle size increases with increasing horizontal force. The particles collected during the tests were analyzed to determine the proportions of tire and road material. According to the results, the tire contributes only about 20% of the particle mass, while 80% is attributable to the road surface. In terms of volume, these shares are 32% and 68%, respectively.



**Citation:** Schläfle, S.; Unrau, H.-J.; Gauterin, F. Influence of Longitudinal and Lateral Forces on the Emission of Tire–Road Particulate Matter and Its Size Distribution. *Atmosphere* **2023**, *14*, 1780. <https://doi.org/10.3390/atmos14121780>

Academic Editors: Yuesen Wang, Xingyu Liang and Ye Liu

Received: 20 October 2023

Revised: 24 November 2023

Accepted: 28 November 2023

Published: 1 December 2023



**Copyright:** © 2023 by the authors. Licensee MDPI, Basel, Switzerland. This article is an open access article distributed under the terms and conditions of the Creative Commons Attribution (CC BY) license (<https://creativecommons.org/licenses/by/4.0/>).

## 1. Introduction

As part of the new Euro 7 emission standards, in addition to emissions from internal combustion engines [1], the European Commission plans to regulate abrasion emissions for the very first time. Conventional friction brakes and the contact between tire and road are primarily accountable for the release of these particulate pollutants. In addition, particles that have already been deposited are resuspended when following vehicles pass, thereby also contributing to air pollution. Timmers and Achten [2] state that particulate matter (PM) from non-exhaust emissions had already accounted for over 90% of total PM emissions from the transportation sector in 2016. According to the current draft of the emission standards, a limit is to be set for brakes that addresses particulate emissions, while for tires, only total abrasion is to be limited [1]. The different kinds of limit values for brakes and tires can be explained by the equally different level of knowledge, which is significantly more advanced for emissions from brakes. Nevertheless, the limit for tire abrasion is most likely only the prelude to increasingly stringent regulations which, in the long term, will also include particulate emissions from the tire–road contact. As fleet electrification progresses, conventional friction brakes will become less important in terms of particulate emissions, so that the tire–road contact will be the last remaining significant source of PM, as long as indirect emissions through resuspension are not taken into account. However, there is currently no reliable database for defining a particulate limit from the tire–road contact,

nor is there a standardized measurement method that could be used to determine the data required. In contrast to the brake unit, this emission source cannot be easily encapsulated, so the investigation is more complex. Previous scientific work investigating this question can be divided into three categories according to their approach [2].

In ambient, roadside, or tunnel measurements [3–11], PM gets collected over an extended period of time. Knowing the particle concentrations at both locations or at both ends of the tunnel, as well as the background concentration, an emission factor (EF) can be derived. This EF can in turn be divided into a combustion and an abrasion fraction by chemical analysis and subsequent apportioning. Statements about individual driving conditions, vehicle characteristics or tire types are not possible or are subject to great uncertainty.

In mobile on-board measurements [2,12–17], a vehicle or a trailer is equipped with measurement and sampling systems. It is driven under various load conditions while emitted particles are measured and collected in the wheel arch. With an additional measurement spot in front of the vehicle measuring the background concentration, its influence and thus fluctuations from the environment can be minimized, but not completely eliminated. Changing wind directions as well as inconsistent flow conditions are disturbance factors and thus reduce the reproducibility. This applies in particular to the requirement for isokinetic sampling, which cannot be guaranteed under changing flow conditions. Furthermore, since only a partial flow at one or several spots behind the tire gets analyzed, reliable conclusions cannot be drawn about the relationship between specific driving conditions and the overall emission. This would require capturing the entire air flow from the contact patch between the tire and the road, mixing it into a homogeneous flow, and sampling a partial flow for analysis. Because of the narrow installation space and the movements of the wheel, this method is particularly challenging. The influence of individual driving parameters can thus be approximated, but not determined precisely. In addition, there are further fluctuations due to particles deposited on the road surface, which are resuspended by rolling over. Clear conclusions about the current total emission from tire–road contact can therefore not be drawn, which hampers the calculation of EFs.

In road simulators or laboratory measurements, one [17–21] or several [5,22–26] tires roll on a drum or circular surface under defined boundary conditions. These tests provide the opportunity of influencing the ambient conditions and thus reach a better reproducibility. This applies in particular to isokinetic sampling, which can be ensured by defined and constant flow conditions. Furthermore, test benches offer the possibility of stationary driving conditions (no mutual influence of single parameters), so that more reliable statements on the emission can be made. For test benches, the diversity of load conditions varies widely. Some only permit a restricted number of parameters (e.g., speed), while in others, no real road surfaces such as asphalt or concrete can be used. Both demands, real road surfaces and free choice of all driving parameters, can be reached with an internal drum test bench. Investigations of PM emissions on internal drum test benches have been presented in Foitzik et al. (2018) [21] and Schläfle et al. (2022, 2023) [27,28] for the nano and the micro range, respectively.

In [28], the used internal drum test bench and its equipment for measuring PM emissions, the procedure for the tests and the processing of the raw data have already been described. Initial findings regarding the correlation between horizontal tire forces and the total emission as well as the particle size distribution were presented. However, it turned out that the number of load conditions was not sufficient to determine a precise correlation between the forces and the emission. This study deals with the performance of the same kind of test bench measurements in order to be able to establish quantitative correlations between longitudinal and lateral tire forces and PM emissions. EFs are calculated for specific driving conditions, from which in future works an average value for complete and real driving cycles can be derived. Also, this study reveals new findings with regard to the particle composition and morphology based on subsequent analyses of the particles collected.

## 2. Materials and Methods

All test series performed in this study were carried out at the internal drum test bench of the Institute of Vehicle System Technology (FAST) at the Karlsruhe Institute of Technology (KIT).

### 2.1. Tire Internal Drum Test Bench

The internal drum test bench (see Figure 1) consists of two subsystems: the drum with an inner diameter of 3.8 m and the sled, on which the tire as well as all systems to measure the forces and torques in the tire-road contact are mounted. The drum is arranged vertically and the tire runs at its lowest point. The two subsystems are driven separately by a 310-kW-engine each; the drum works electrically while the drive and all movements of the wheel are powered hydraulically. The separate propulsion allows for the investigation of both stationary and realistic driving conditions. If, in addition to the vertical load, no other forces are acting, the tire and drum turn at the same speed (free rolling). As they are driven separately, longitudinal slip conditions, i.e., drive and brake slip causing longitudinal forces, can be adjusted stationarily and reproducibly. In order to apply lateral forces the sled rotates around the vertical axis of the wheel causing a slip angle and thus lateral slip. The test bench can be equipped with several surfaces, including safety walk as well as real road surfaces, such as asphalt and concrete, which enables an exact replication of the tire-road contact on the open road. A widely used asphalt mix AC 11 D S was used in the tests for this study. This is asphalt concrete with a maximum grain size of 11 mm. The majority of the added aggregate is moraine, which was mixed with bitumen as a binder in a ratio of about 95% to 5% by mass. The entire test bench is surrounded by an enclosed chamber, which allows the minimization of fluctuations of background concentration. The ambient temperature can be adjusted in a range between  $-15^{\circ}\text{C}$  and  $35^{\circ}\text{C}$ .

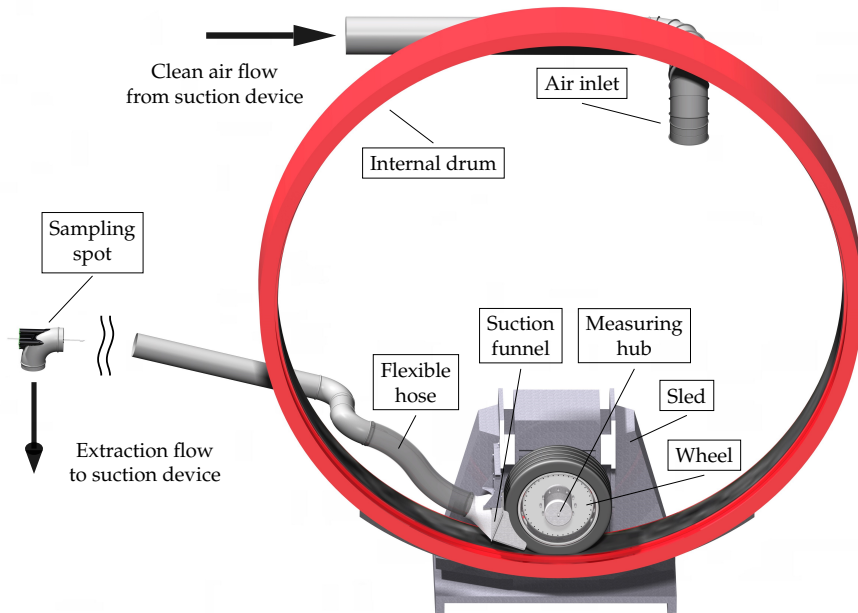


**Figure 1.** CAD representation of the internal drum test bench at FAST/KIT with the components extended for the measurement of tire-road particulate matter. For better visibility of the components, the back panel of the internal drum as well as the front fairing are not shown.

### 2.2. Sampling and Measuring

To investigate PM emissions from the tire-road contact a suction funnel is installed directly behind the tire (see Figure 1). It is mounted on the test bench sled and thus follows the wheel's movements when cornering. The suction funnel is adaptable to a wide range

of tire diameters and widths and encloses the rear part of the tire at an angle of about 70°, leaving only a narrow slit of about 10 mm. It is connected to a spiral hose ( $\varnothing$  160 mm), whose flexibility is required to allow for the investigation of lateral forces due to slip angle. The opposite end of the spiral hose is connected to a spiral duct ( $\varnothing$  160 mm), eventually leading to the suction device. Metal tubes are used to prevent losses due to electrostatic charge, and the flexible spiral hose is made of permanently antistatic polyurethane. In addition, the ends of the copper wire inside the wall of the spiral hose are grounded.

The suction device (ESTA DUSTOMAT 4–10 eco<sup>+</sup>, Senden, Germany) vacuums the particles emitted in the tire–road contact. The sampling spot is integrated into a bend of the spiral duct which is passed by the flow on its way from the tire to the suction device. Due to the sampling through a bend, a straight sampling tube can be used, which subsequently minimizes particle losses due to sedimentation. A partial flow of 5 L/min is taken isokinetically based on ISO 9096:2017 [29] at the sampling spot. The aerosol is analyzed by a light-scattering aerosol spectrometer system (PALAS Promo 2000 & welas 2500, Karlsruhe, Germany), which can detect particles in four different size ranges from 0.2  $\mu\text{m}$  to 100  $\mu\text{m}$  [30,31]. As the focus of this study is on the determination of PM emissions, the size range between 0.3  $\mu\text{m}$  and 17  $\mu\text{m}$  was selected for all tests, of which only those particles with a diameter of less than 10  $\mu\text{m}$  were taken into account for the evaluation. The measuring rate can be set to a maximum of 1 Hz. In addition to assessing the level of emission, the high measuring rate enables statements about the size distribution during individual load conditions (longitudinal and/or lateral force). To obtain meaningful and reproducible results, the aerosol spectrometer must be calibrated regularly with calibration dust (PALAS MonoDust 1500, Karlsruhe, Germany). The aerosol spectrometer system detects the scattered light pulse of each particle which crosses the control volume. Based on this, a particle diameter is assigned to each particle assuming its refractive index and aspect ratio. Refractive index and aspect ratio in this study were chosen to be 1.59 and 1, respectively, which corresponds to spherical particles (see Section 3.5). Furthermore, a density of 2.299 g/cm<sup>3</sup> was assumed to convert particle size into particle mass (see Section 3.5). Besides the port for sampling the aerosol, the sampling apparatus has further ports to insert a dynamic pressure anemometer. The resulting monitoring of the flow velocity ensures isokinetic sampling during the tests. The necessary condition of a homogeneous extraction flow is ensured by high turbulence in the suction duct.

The remaining aerosol reaches the suction device, where it undergoes a three-stage filtration. Coarse particles are separated from the air flow by an impact separator and fall into a dust collection box. Finer particles reach the cartridge filters and are separated there. Due to the regular self-clearing of the filters using the jet pulse process, these particles also end up in the dust collection box. The remaining particles reach the fine dust filter (HEPA-14) and are eventually separated from the air flow, so that the air after this filter no longer contains any notable number of particles.

The suction device generates a maximum volume flow of 2000 m<sup>3</sup>/h. The extraction system has a second inflow through which air from the environment is sucked into the suction device. This can be adjusted as required. The additional air flow from the environment means that more air flows into the drum than is extracted behind the tire. The resulting overpressure ensures that contamination of the measurement by particles from the ambiance can be avoided.

The secondary inflow was set to 400 m<sup>3</sup>/h for this test series, so that the extraction volume flow from the drum was 1600 m<sup>3</sup>/h. This combination was chosen to reach a flow velocity of at least 120 km/h in the slit between the tire and the suction funnel. Therefore, it can be assumed that emitted particles are reliably extracted for all driving conditions in which the driving speed and the resulting flow velocity inside the drum are lower than this value. Presuming that all particles are extracted, the total emission of the tire–road contact can be concluded using the particle concentrations measured by the aerosol spectrometer.

More detailed information on the internal drum test bench at KIT as well as on the equipment and the extensions for PM emission measurements, can be found in [27] or [28].

### 2.3. Varied Parameters

All tests were conducted with a premium summer tire of the dimension 255/40 R20 with a load index of 101. This tire type is suitable for passenger cars of the F-segment or luxury class. In order to keep the environmental conditions as constant as possible, the ambient temperature was kept at 25 °C by an air conditioning system. The focus of the study was on quantifying the emission of PM when applying longitudinal and lateral forces, so only these parameters were varied (see Table 1). To enable accurate conclusions to be drawn about the emission under specific load conditions, they were set and held stationary for several seconds, allowing for a meaningful emission value for one particular load condition. The remaining tire and chassis parameters (see Table 1) were kept constant throughout the test and are subject to future experiments.

**Table 1.** Varied as well as constant parameters with the respective values.

	Parameter	Parameter Values
Varied	Longitudinal force $F_x$	0 kN;
	Lateral force $F_y$	±1 kN; ±2 kN; ±3 kN; ±4 kN
Constant	Vertical load $F_z$	6.5 kN
	Speed $v$	80 km/h
	Inflation pressure $p_i$	2.6 bar
	Camber angle $\gamma$	0°
	Ambient temperature $T_a$	25 °C

Figure 2 shows the matrix of all investigated combinations of longitudinal and lateral forces. A pure load of 4 kN longitudinal or lateral force corresponds to an adhesion utilization  $F_x/F_z$  or  $F_y/F_z$  of 0.62 with the underlying vertical load of 6.5 kN. For combined forces, the adhesion utilization can be calculated by  $F_{res}/F_z$ . If all four tires of a real vehicle had an adhesion utilization of 0.62, a longitudinal, lateral, or combined acceleration of approximately  $6 \text{ m/s}^2$  (0.62 g) would result. For conventional drivers and vehicles, this value is already within the threshold range of driving dynamics, so that the resulting emissions are of minor importance for an average driving style. Furthermore, average drivers do not use combinations of extreme longitudinal and lateral force, so no load combinations outside the diagonal between the maximum pure longitudinal and lateral forces were tested. The load conditions illustrated in black in Figure 2 are used in later sections to create regression models that specify the emission as a function of the respective load type (longitudinal forces, lateral forces, combined forces). The load conditions illustrated in gray are used to validate these regression models.

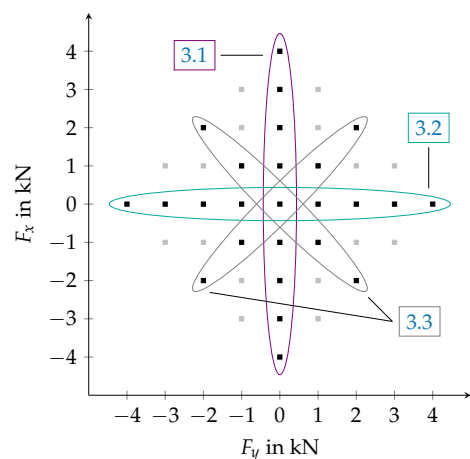


**Figure 2.** Overview of the load matrix comprising 40 (41 with free rolling) different load conditions.

## 2.4. Experimental Setup and Procedure

To remove the outermost layer of the tire and thus to exclude associated non-representative emissions from the particle measurements, the tire first underwent a running-in process. Afterwards, aiming to ensure high reproducibility due to constant ambient temperature, the air conditioning system was turned on several hours before the test runs started.

Also, for higher reproducibility, all load conditions were applied several times. However, they still caused different results. This was an indicator for changes taking place on the road surface. Preceding tests had shown that its condition already changes during single test runs which in turn influences the amount of PM emitted. The roughness of the road surface, or more precisely its skid resistance and thus its abrasiveness, decreases as the tire is constantly driven over. This polishing effect also occurs on open roads. Due to the limited length of the drivable track in the test bench, however, it is much faster here. Various methods did not help to stop or slow down the change in the condition of the road surface. Therefore, the condition of the road surface had to be considered as an additional parameter when conducting the tests, as well as for the subsequent analysis of the data. To this end, eight test passages, each of them consisting of four test blocks, were performed (see Figure 3). During each test block, all load conditions shown in Figure 2 were approached exactly once. The sequence of load conditions was varied between the test blocks, so that an influence of the order on the emission can be ruled out. A regenerating process of the road surface was performed at the beginning of each test passage to make sure that each load condition was performed on every road condition. Regeneration was done by driving a studded tire under slip angle, which mainly increases the micro roughness and thus reverses the polishing effect caused by the constant rolling-over. The micro roughness of the road was determined before, in between, and after the test blocks, measuring the SRT value with a portable skid resistance tester (SRT, Munro-Stanley London, Harlow, United Kingdom), as regulated in EN 13036-4:2011 [32].

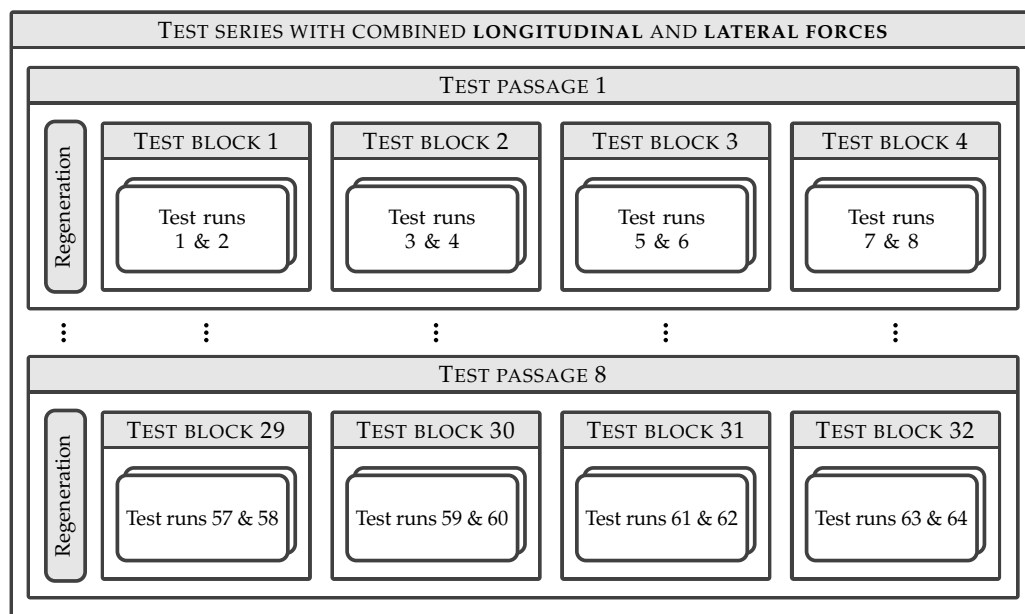


**Figure 3.** Overview of the test series consisting of 8 test passages with 8 single test runs each.

The experimental procedure described in the following two paragraphs has already been used in a former study by Schläfle et al., and is therefore basically taken over [28].

The individual test runs were carried out according to a fixed procedure. At the beginning, the tire was driven until it had reached a surface temperature of 28 °C. To prevent the tire surface from becoming tacky, a sand mixture of quartz, corundum and calcium carbonate was then added as third-body material. Earlier tests had revealed that a complete lack

of dirt between the tire and the road changes the surface of the tire, thus totally impeding the release of fine tire and road wear particles (TRWP). As soon as the surface gets tacky, the majority of the generated particles keep sticking to the tread and do not leave the tire anymore. The particles being released despite the stickiness of the tire are disproportionately large compared to those generated on the open road and are therefore not representative. This effect can be avoided by adding third-body material periodically. In order to not contaminate subsequent particle measurements of the aerosol spectrometer system the decisive factor is to choose a third body whose lower threshold in size distribution is larger than the coarsest particles to be measured. When adding the sand, the driving speed was decreased to 50 km/h and the suction device was switched off in order to prevent the sand from being swirled around too much by the air flow in the drum. After 5 min, in which the sand was able to act in tire–road contact, the suction device was switched on again to suck off the previously added sand. To start a test run, it was then waited until both the particle number concentration (PNC) and the particle mass concentration (PMC) had declined to the level that had been present before the sand was added.

In one test block, there were two single runs of 24 individual load conditions each (see Figure 4). The first four were aimed at whirling up and vacuuming the sand remaining in the drum and were not considered for later analysis. The 20 subsequent load conditions were composed of different longitudinal and lateral forces (see Figure 2) and were used for later evaluation. To prevent the tire temperature from rising unrealistically high, there was always a phase between two load conditions in which the tire rolled freely (only vertical load) or was even lifted (no vertical load). Furthermore, when determining the sequence of load conditions, care was taken to ensure that the load directions always alternated. This prevented the tire from adapting to the load direction, which had led to decreasing emissions in preliminary tests. Therefore, combinations in which the longitudinal and lateral force pointed into the same direction never followed each other.

In total, 64 individual test runs were carried out, eight test passages of eight single runs each. The forces in all three spatial directions were controlled, while the other variables were held constant. Both particle concentrations were recorded during the entire test series.

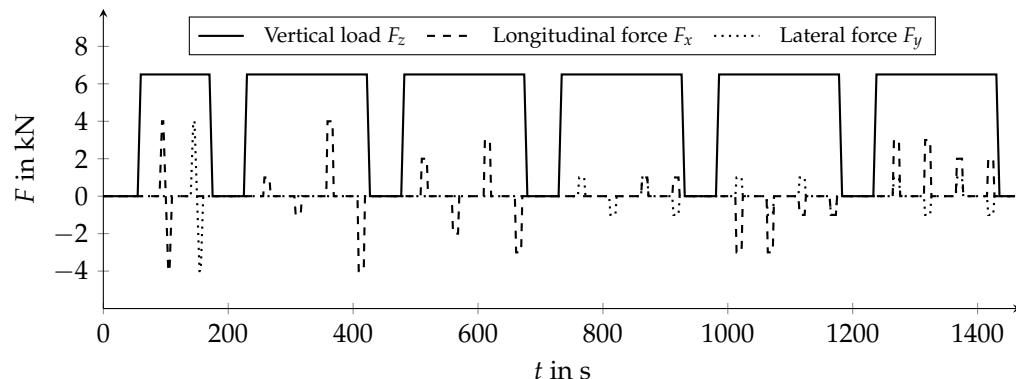


**Figure 4.** Exemplary test run with four initial load conditions to whirl up sand remaining on the road surface and 20 subsequent load conditions comprising longitudinal and lateral forces.

## 2.5. Data Processing and Evaluation

For data processing and evaluation, the same method was applied which had been developed and described in detail in [28]. Thus, it is presented in condensed form here.

Based on the raw emission data of PMC and PNC, an average emission value was calculated for each load condition (load conditions 5 to 24) from Figure 4. The background concentration which had already been present before applying the load, was subtracted from this emission value, so that the obtained value corresponds to the net emission caused by exclusively this load.

The skid resistance of the pavement was determined before, between, and after the individual test blocks. A standard curve for the course of the SRT value during one test

passage was derived from all measurements. Using this curve, it was possible to assign the currently present SRT value to each load condition and thus to link load, SRT value, and emission (PMC and PNC) to form a data triplet. Using the data triplets, regression models for the relationships between emission and SRT value at constant loads were derived. For the final results of this study, an SRT value of 60 was selected which corresponds [33] to the acceptance value for new road surfaces [34] recommended by the German Road and Transportation Research Association (Forschungsgesellschaft für Straßen- und Verkehrswesen, FGSV). The emission values at this SRT value were calculated from the regression models and plotted over the respective load type.

For more detailed information about data processing, see [28].

### 3. Results

The particle concentrations (PMC and PNC) measured in the particle size range between 0.3  $\mu\text{m}$  and 10  $\mu\text{m}$  at the internal drum test bench during the tests are characteristic of this test bench setup and cannot be directly compared with the results of other test benches or driving on real roads. For this purpose, emission factors are required, which describe the emission of a vehicle per distance traveled (unit: mg/vkm or #/vkm), independent of the measurement method.

Emission factors can be derived from the measured particle concentrations. For this purpose, it is assumed that all particles emitted in the tire-road contact were extracted by the extraction flow. Furthermore, it is assumed that the aerosol sampled for measurement was representative of the total extraction flow. Under these conditions, and considering the extraction volume, the total mass or total number of emitted particles can be calculated. By dividing the value by the speed driven, the reference quantity changes from time traveled to distance traveled. In order to obtain the emission factor for a whole vehicle, the value is multiplied by the number of wheels, which was set to four for all tests in this study.

#### 3.1. Influence of Longitudinal Forces

In Figure 5, the influence of the longitudinal force on the mass-based (Figure 5a) as well as on the number-based emission factor (Figure 5b) is shown. The single data points were obtained from the data evaluation described in Section 2.5. In addition, two different regression models are plotted to best show the quantitative relationship between emission and longitudinal force.

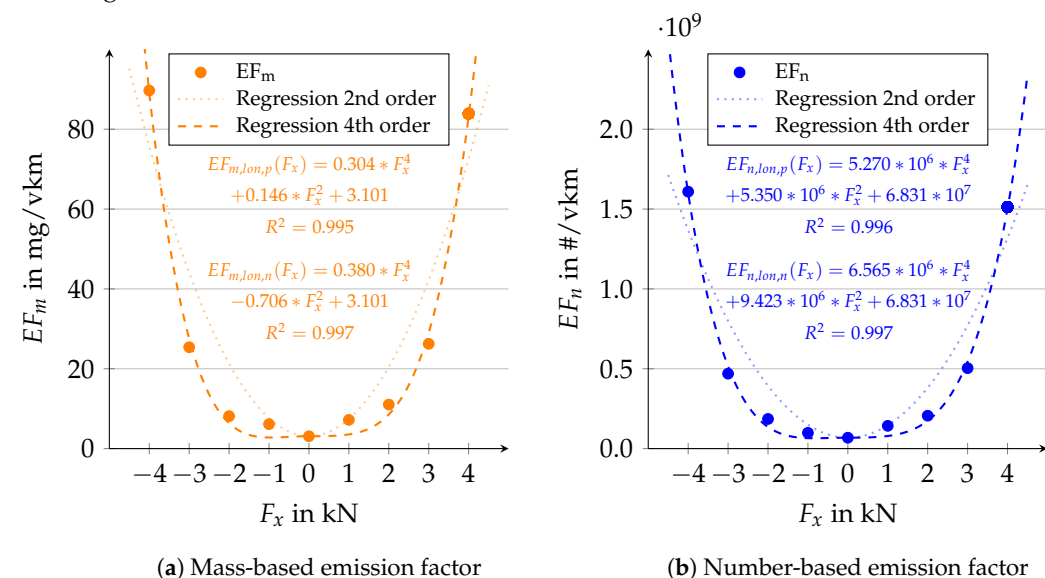


**Figure 5.** Calculated values for emission factors in the size range between 0.3  $\mu\text{m}$  and 10  $\mu\text{m}$  at individual load conditions and different regression models versus longitudinal force for a summer tire at an SRT value of 60.

For both particle mass and number, it is apparent that the emission only increases weakly at moderate loads, but that this increase significantly amplifies with higher loads, resulting in progressive increases. The weak increase in emission at low loads may be due to the predominant deformation slip present. The individual tire tread blocks are deformed in longitudinal direction as they pass through the tire–road contact, but do not reach the adhesion limit until the end, and therefore return to their original position when they leave the contact area. At higher loads, however, they reach the adhesion limit, so that gliding slip occurs, which could be responsible for the sharp rise in emission values.

Furthermore, it can be seen that the values for the emission factor of braking and driving are not completely axisymmetric. At negative longitudinal forces, i.e., braking, the summer tire investigated appears to emit more particles than at comparable driving forces. A possible explanation for this difference could be the shear stress distribution in the tire–road contact area, which is adverse for braking, meaning that the adhesion limit is reached earlier for braking than for driving. This, in turn, results in more gliding and less deformation slip, which enhances the generation of tire wear and thus PM emissions.

To determine the quantitative dependence of the emission on the longitudinal force, the emission values were approximated using a quadratic and a fourth-order regression function. To achieve the best possible result, positive ( $p$ ) and negative ( $n$ ) longitudinal forces were evaluated independently of each other. The regression functions were determined with the constraint of passing through the emission value for free rolling ( $F_x = 0$ ). For both particle mass and number, the quadratic approaches are found to approximate emissions well for moderate forces, but to deviate significantly as the force increases. This contrasts with the fourth-order approaches, which initially underestimate the emission, but appear to represent the progression at higher loads much more accurately. Because of the apparent superiority of fourth-order regressions only their functions are given and the quadratic functions are shown partially transparent. All subsequent calculations are based on the fourth-order regression functions.

### 3.2. Influence of Lateral Forces

The result on the influence of lateral forces on the emission is shown in Figure 6. The measurements have shown a difference in emission between positive and negative lateral forces. Since this difference has also occurred with other tire models, and positive lateral forces have always led to the higher emissions, it can be assumed that this effect is more likely caused by the test bench itself and is not an actual direction-dependent emission behavior.

The plausibility of this assumption can be evaluated by a more detailed analysis of the test bench structure and its function. At the internal drum test bench, positive lateral forces correspond to driving a left-hand curve. In this case, the flow prevailing in the test bench hits the right outer side of the wheel, thus ensuring that the extraction flow is further intensified and that emitted particles are blown into the suction funnel. In the case of negative lateral force, the wheel is driving a right-hand curve. The flow hits the left outer side of the wheel. The difference, however, is that the flow on this side is slowed down by the non-rotating components (front fairing, portal, sled) and hampers the amplification of the extraction velocity. Emitted particles could thus be extracted less reliably and enter the drum environment. Since no reliable statement can be made about the difference between the emission for positive and negative lateral forces due to this test bench behavior, only mean values of both force directions are shown.

For both particle mass (Figure 6a) and particle number (Figure 6b), the same statements apply as for longitudinal force: At moderate force, there is a weak increase in emission, which intensifies as the force increases. The growing influence of gliding slip is probably responsible for this, as outlined in Section 3.1. Again, the fourth-order regression functions describe the emissions more accurately than the second-order functions. The comparison of the emissions at longitudinal and lateral forces reveals that the absolute values for lateral forces are about a factor of four higher than for longitudinal forces.

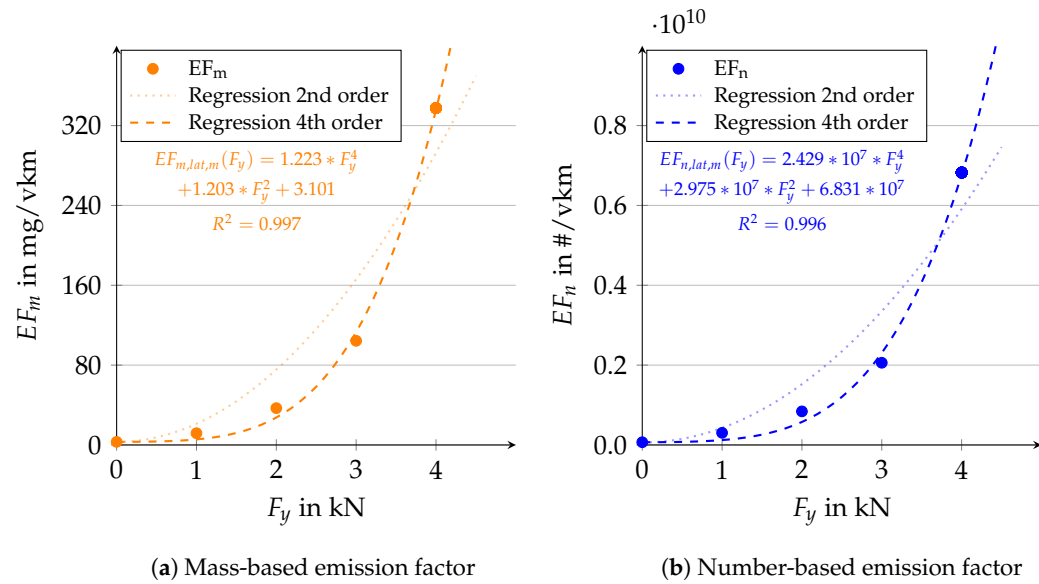


**Figure 6.** Calculated values for emission factors in the size range between  $0.3\text{ }\mu\text{m}$  and  $10\text{ }\mu\text{m}$  at individual load conditions and different regression models versus lateral force for a summer tire at an SRT value of 60.

One possible explanation is the summer tire's tread design. It has mainly longitudinal grooves, but hardly any lateral sipes and no lateral grooves. This means that the tread ribs are almost continuous in the longitudinal direction and tread edges only run longitudinally. When loaded with longitudinal force, the missing lateral grooves and sipes may result in less deformation and edge wear. When loaded with lateral force, however, the ribs are deformed laterally to their direction of propagation, with greater deformation as well as increased edge wear, thus favoring overall emission.

### 3.3. Influence of Combined Forces

In order to see how load conditions comprising longitudinal and lateral force affect the emission compared to pure forces in the longitudinal or lateral direction, emission factors are also plotted over the resulting force (see Figure 7). Since the effect of direction-dependent emission described in Section 3.2 was also present here, only one course is shown. It represents the mean values of the emission of all four diagonals shown in Figure 2. This means that only conditions were considered in which the longitudinal and the lateral force were equal in magnitude.

The statements made for pure longitudinal and lateral force with respect to the slopes and approximation also apply here, although the differences between second- and fourth-order regression functions are smaller due to the small number of support points. This also explains why the coefficient of determination is 1. However, it is also clear that the quadratic regression overvalues the emission at 2 kN. This effect has already been described in a former study, in which only three support points were available to approximate the functions at positive and negative horizontal forces, respectively [28]. However, from Sections 3.1 and 3.2, it is now obvious that fourth-order functions approximate the emissions much better. Thus, it can be assumed that the PM emission increases with the fourth order as a function of the force, independent of its direction.

To compare the absolute values for different types of loads, the previously determined emission curves are plotted together in Figure 8. It can be seen that lateral forces lead to by far the highest emissions and that combined loads, consisting of equal parts of longitudinal and lateral force, are between the two pure loads. It should be noted, however, that at high load the support range of the regression function for combined forces is exceeded, so that these values must be interpreted with a particular degree of uncertainty.

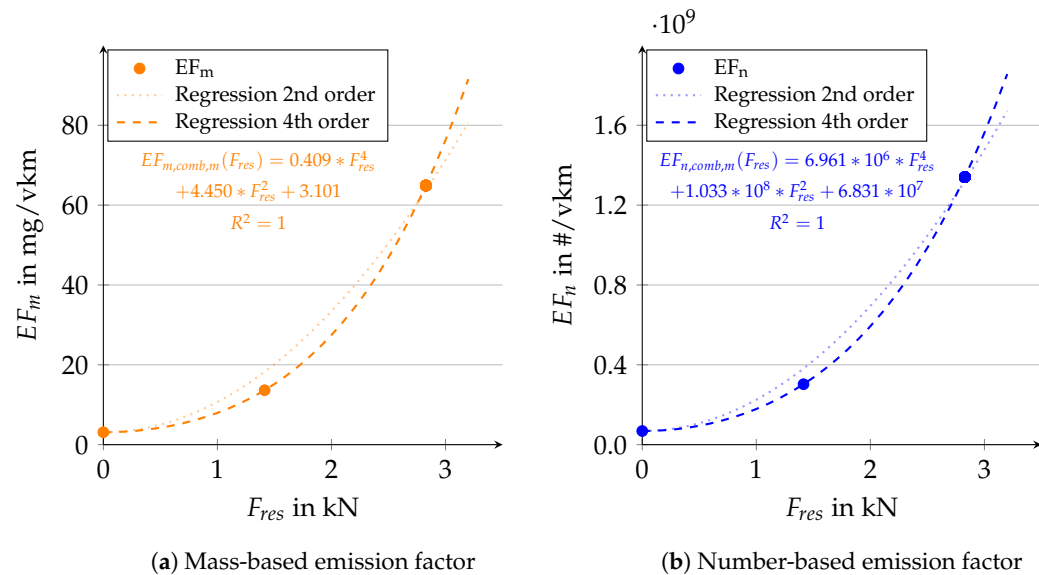


**Figure 7.** Calculated values for emission factors in the size range between  $0.3\text{ }\mu\text{m}$  and  $10\text{ }\mu\text{m}$  at individual load conditions and different regression models versus combined force for a summer tire at an SRT value of 60.

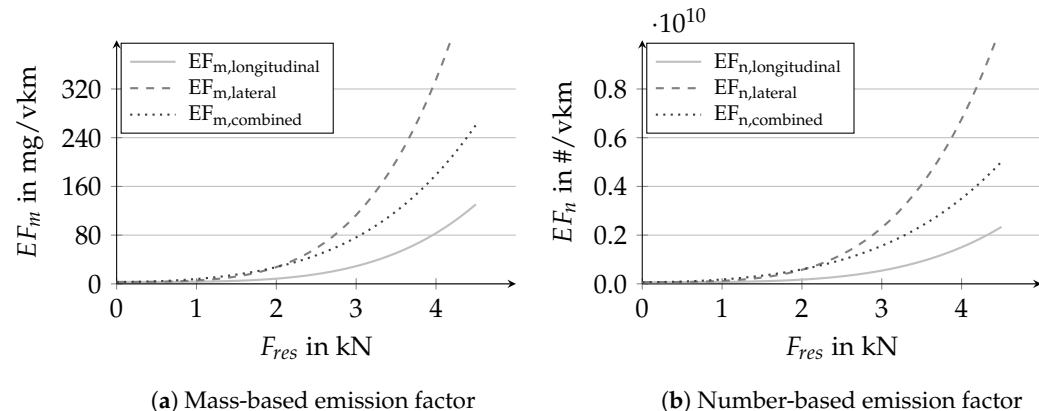


**Figure 8.** Calculated courses of emission factors for pure longitudinal and lateral forces as well as combined forces for a summer tire at an SRT value of 60.

Based on the regression functions for the emission when loaded in different force directions, a general function was calculated, which approximates the emission for the entire range of horizontal tire–road contact forces. Due to the different emission behavior for driving and braking (see Section 3.1), the function was approximated for each quadrant separately. Since the target function is a surface created by rotation around the vertical axis, polar coordinates were used and pure driving forces correspond to an angle of 0. Since all predetermined functions (longitudinal, lateral, and combined) are fourth-order polynomials with exclusively even exponents, they can be described with the generally valid function given in Equation (1). The transition between the individual predetermined functions was achieved by gradually converting the respective factors into each other using fourth-order polynomials for  $a(\varphi)$  and  $b(\varphi)$ , where  $\varphi$  represents the angle between positive longitudinal direction and the resulting force acting on the tire. The surface spanned by the three-dimensional regression function for the mass-based EF is shown in Figure 9.

$$EF_m(F_{res}, \varphi) = a(\varphi) * F_{res}^4 + b(\varphi) * F_{res}^2 + c \text{ for } F_{res} \geq 0, 0 \leq \varphi < 2\pi \quad (1)$$

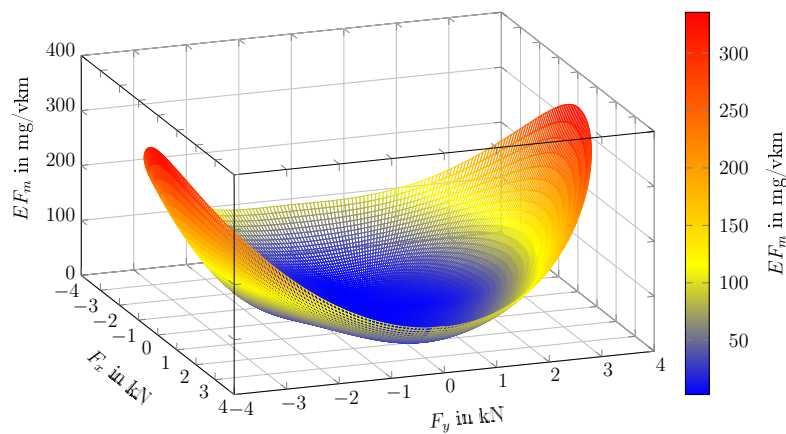


**Figure 9.** Calculated courses of mass-based emission factors for all horizontal forces in the tire–road contact for a summer tire at an SRT value of 60.

The facts described in the sections above become even clearer here: moderate emissions are generated at low loads. With increasing load, the emission increases strongly. This increase is particularly pronounced for lateral forces, resulting in a significant increase on both sides of the surface. In Figure 10, the resulting surface is shown in plan view. It can be seen that a circle with the radius of the maximum force applied results when the surface is projected onto the base surface. In addition, the measurement points which were not used for determination of the regression models (see Figure 2) are shown as individual data points for validation. Since no distinction was made between positive and negative lateral forces when the model was created, the validation points displayed also represent the mean values of the emission when loaded with positive and negative lateral forces in each case. Based on the color, it can be seen how precisely the model predicts the emission for each condition. Only for the loads with  $\pm 3\text{ kN}$  longitudinal force does the model underestimate the actual emission. This fact suggests that the influence of the lateral force is even greater than assumed by the model, so that the emission increases immediately even if only a low lateral force is applied in addition to the longitudinal force.

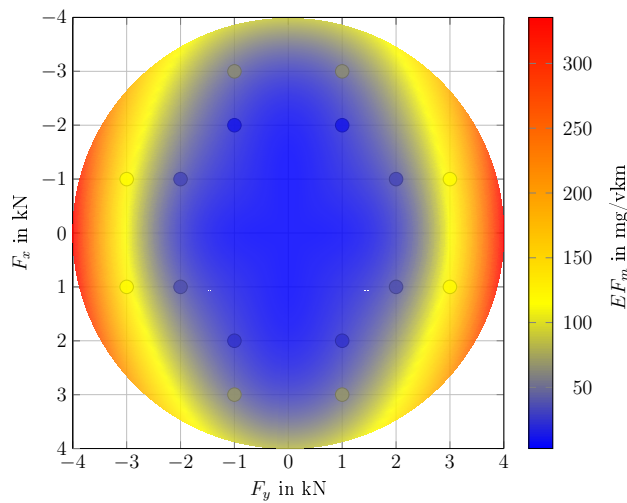


**Figure 10.** Visual validation of the model using the load conditions which had not been used for the determination of the model.

This inaccuracy is also evident from Table 2, in which absolute as well as relative discrepancies are shown. For the relative deviations, it should be noted that the highest emission factor occurring was used as reference value. For all conditions, the percentage deviations remain in a low range. Even for the quite high absolute deviations in the range of 10 mg/vkm, the relative deviation is low, indicating satisfactory accuracy of the model.

**Table 2.** Differences between the emissions calculated by the model and the measured ones.

$F_x$ in kN	$F_y$ in kN	$\Delta EF_m$ in mg/vkm	$\Delta EF_m$ in %
3	1/-1	-18.98	-5.66
2	1/-1	0.22	0.07
1	2/-2	3.72	1.11
1	3/-3	12.11	3.61
-1	3/-3	10.29	3.05
-1	2/-2	6.77	2.02
-2	1/-1	10.29	3.07
-3	1/-1	-18.69	-5.57

The shown emission characteristics results from the investigations with one summer tire model. However, investigations with other summer tires have shown similar emission behavior with regard to the difference between longitudinal and lateral forces, so that general validity can be assumed for the course of the curve. Since the mass-based particulate matter emission was the focus of this work, only the associated emission factor is shown. Analogous to the described procedure, however, a map for the number-based emission factor could also be created.

### 3.4. Influence of Load Conditions on the Particle Size Distribution

A close comparison of the percentage increases in the EFs of particle mass and number in Sections 3.1 and 3.2 reveals that the emissions increase to different extents. While there is a factor of about 28 between the emitted particle mass in the freely-rolling state and that at maximum longitudinal force, this factor is only 23 for the emitted particle number. For lateral forces, the factors between emission with a freely-rolling wheel and loaded with the maximum force of 4 kN are 109 for the particle mass and 99 for the particle number. In both cases, the different increases in emission factors indicate that the emission does not only increase, but that there is also a shift in size distribution toward larger particles.

For a more detailed investigation of the influence of load on the particle size distribution, the size distributions of several time steps during one test run were combined to form more meaningful courses. In this way, an individual particle size distribution was determined for each load condition, which contains the size distributions from all measurement programs in which this load had occurred. The particle mass distributions for four load conditions consisting of pure longitudinal force are shown in Figure 11.

The differential distributions increase with higher load, meaning that the total emission increased with increasing longitudinal force. The proportion of the total emission grows with increasing particle diameter, resulting in a rising edge on the right-hand side of the diagram. From the cumulative distributions, it is evident that larger particles are increasingly generated with higher longitudinal force, so that the size distribution shifts to the right. This effect was also observed by Park et al. (2018) [20] with increasing load. The reason for the generation of larger particles is probably the higher shear stress in the contact area between tire and road due to the higher force. This could lead to increased and more intense formation of cracks, which favors the generation of larger particles. Moreover, higher shear stress results in a higher proportion of gliding slip and thus in higher heat input into the tire. Due to the higher temperature, the tire material becomes softer and the total tire wear increases. Since most of the emitted mass is caused by large particles and the resolution of the ordinate is small as a result, it is not clear from this diagram whether there are also changes taking place in the range of smaller particles ( $d_p < 1 \mu\text{m}$ ). For this purpose, the particle number distributions of the same load conditions are shown in Figure 12.

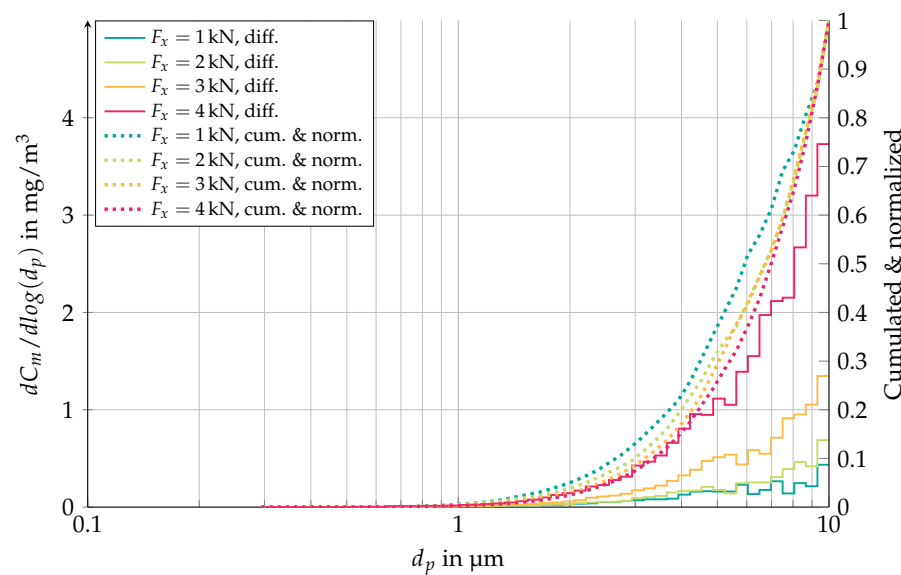


**Figure 11.** Particle mass distributions for longitudinal forces applied to a summer tire.

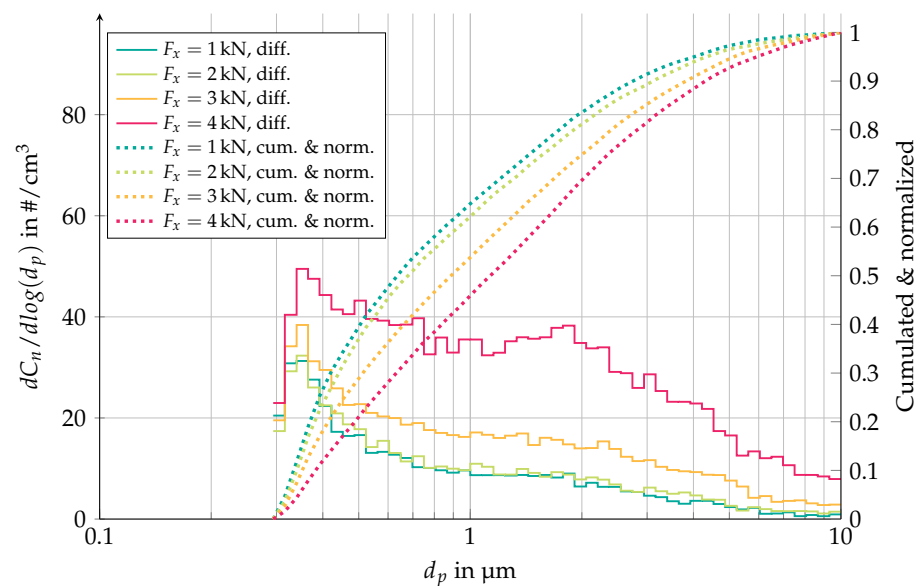


**Figure 12.** Particle number distributions for longitudinal forces applied to a summer tire.

The particle mass no longer plays a role in this representation, so that the range of smaller particles is better visible. In this plot, a bimodal distribution can be seen with the upper peak at about  $1.8 \mu\text{m}$ . There must be a second peak below the lower detection limit of the aerosol spectrometer, so that a rising edge is indicated at the left edge. The lower particle abundance in the smallest two size channels can be attributed to decreasing counting efficiency of the aerosol spectrometer towards the lower detection limit. Furthermore, it can be seen that an increase in emission with increasing longitudinal force also takes place in this range, even if it is less pronounced in percentage terms compared to the range of larger particles. The shift towards larger particles is again apparent from the cumulative distribution. For the longitudinal forces from  $1 \text{ kN}$  to  $4 \text{ kN}$ , the value of 50% of the total number of particles is reached at  $0.59 \mu\text{m}$ ,  $0.63 \mu\text{m}$ ,  $0.84 \mu\text{m}$ , and  $1.06 \mu\text{m}$ , respectively, indicating the shift in particle size distribution.

For lateral forces, comparable trends are obtained for both particle mass and particle number distributions, so the associated graphs are not shown separately.

### 3.5. Particle Composition

The particles picked up by the extraction flow reached the suction device and were separated in one of the three filters. The ones separated by the impact separator or the cartridge filters got deposited in the dust collection box. The total amount of TRWP collected there during the test series was used for analysis. Firstly, the complete sample was weighed using a precision scale. Secondly, the grain size distribution was determined using a cascade of sieves. Thirdly, the individual size fractions obtained were weighed again. The finest sieve for conventional sieving had a nominal size of 40  $\mu\text{m}$ . Since conventional sieving did thus not allow for isolating the size fraction of particulate matter ( $d_p < 10 \mu\text{m}$ ) directly, another way was chosen to determine its density. Therefore, the smallest size fraction available after conventional sieving ( $d_p < 40 \mu\text{m}$ ) was sieved again using an air jet sieve machine, which had a cut diameter of 20  $\mu\text{m}$  and removed particles smaller than that. Due to the method itself, the removed particles were not further available, meaning that eventually only two size fractions were available: one comprising particles smaller than 40  $\mu\text{m}$ , and one with particles between 20  $\mu\text{m}$  and 40  $\mu\text{m}$ . The mass ratio between these size fractions was again recorded by weighing, and is shown in Table 3.

**Table 3.** Mass fractions and densities of different size fractions.

Size Fraction	Size Range	Mass Fraction $M$ in %	Density $\rho$ in $\text{g}/\text{cm}^3$
Total fraction	$d_p < 40 \mu\text{m}$	100.00	2.225
Coarse fraction	$20 \mu\text{m} < d_p < 40 \mu\text{m}$	89.01	2.216
Fine fraction	$d_p < 20 \mu\text{m}$	10.99	2.299

The density of both size fractions was determined using a gas pycnometer (Micromeritics AccuPyc II 1340, Norcross, GA, USA) and measuring several individual samples. Based on the mass ratio between the coarse and the fine size fraction determined by weighing and using Equation (2), the density of the fine fraction ( $d_p < 20 \mu\text{m}$ ) could be calculated (see Table 4).

$$\rho_{Total} = \rho_{Fine} * M_{Fine} + \rho_{Coarse} * M_{Coarse} \quad \text{with} \quad M_{Fine} + M_{Coarse} = 1 \quad (2)$$

The particle fraction smaller than 20  $\mu\text{m}$  does not correspond to the PM<sub>10</sub> fraction, whose density should actually be determined. However, due to the fact that particles in this size range are formed by the same mechanisms, it can be assumed that their density is equivalent as well. The calculated density seems plausible, since it is between the densities of the two components tire tread and road material (see Table 4), which had also been determined using the gas pycnometer. The obtained value for the density of TRWP is slightly higher than in [35,36], where the authors give the upper limit with 2.2  $\text{g}/\text{cm}^3$ . It should be noted, however, that both of these mainly refer to coarser particle fractions, so that density differences are possible and are also indicated in Table 3. Additionally, there are studies that give even higher densities. Gustafsson et al. (2008) [24], Hussein et al. (2008) [13], Aatmeeyata et al. (2009) [18], and Sjödin et al. (2010) [5] use densities between 2.53  $\text{g}/\text{cm}^3$  and 2.8  $\text{g}/\text{cm}^3$  for their calculations.

Using the density, the proportion of the tire and the road could be calculated. For this purpose, it was assumed that when driving on the asphalt surface, the bitumen as well as the aggregates contained therein were abraded according to their share in the road surface (95% aggregate, 5% bitumen). This assumption is corroborated by the fact that the macro roughness and, consequently, the appearance of the road surface did not change over several test series. If high amounts of bitumen were abraded, aggregate breakouts and an increase in macro roughness should have taken place. Conversely, if mainly aggregate were abraded, the result would be a lower macro roughness and an overall smoother appearance of the roadway. Under this assumption, the density of the abraded road material was

calculated (see Table 4). Using this value, the density of the tire tread, and Equation (3), the contributions of the tire and the road to the PM collected could be derived.

$$\rho_{PM} = \rho_{Tire} * M_{Tire} + \rho_{Road} * M_{Road} \quad \text{with} \quad M_{Tire} + M_{Road} = 1 \quad (3)$$

The mass fractions obtained are shown in Table 4. The one of the tire seems to be very small; however, it must be taken into account that the density of the tire tread is significantly lower than the one of the abraded road material. Thus, for a better impression of how large the contributions of tire and road are, the volume fractions of the TRWP were also calculated. The indication of volume fractions allows visual comparison with images. For this purpose, Figure 13 contains two SEM images of TRWP collected during the test series.

**Table 4.** Densities and fractions of materials contained in fine TRWP ( $d_p < 20 \mu\text{m}$ ). The two components shown in gray are the sub-fractions of the road material.

Material	Density $\rho$ in $\text{g}/\text{cm}^3$	Mass Fraction $M$ in %	Volume Fraction $V$ in %
Tire tread	1.206	18.2	32.0
Road material	2.543	81.8	68.0
Aggregate	2.622	77.7	60.0
Bitumen	1.035	4.1	8.0
PM (TRWP)	2.299	100.0	100.0

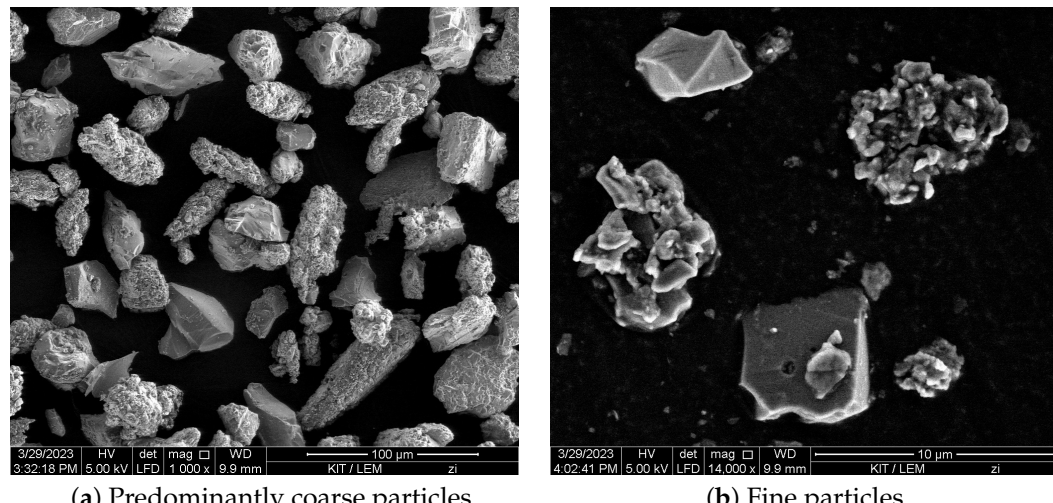


**Figure 13.** SEM images showing particles of different size fractions and different composition collected in the dust collection box of the suction device during the test runs.

Figure 13a shows an overview of particles, most of which are coarse with diameters between  $20 \mu\text{m}$  and  $40 \mu\text{m}$ . It is apparent that particles of different compositions are contained. On the one hand sharp-edged, presumably mineral particles from the aggregates of the road surface. On the other hand, typical elongated TRWP encrusted with smaller minerals, as described in [37]. Since the aggregate material occurs both purely in the form of coarse particles, as well as in the form of tiny fragments within and around the conglomerates, it seems plausible that the aggregate makes up a larger mass and volume fraction. In addition, it must be taken into account that visually, a distinction between tire tread material and bitumen is impossible. Thus, on the images only a common fraction of tire tread material and bitumen can be distinguished from a aggregate fraction, which according to the calculation should account for 40% and 60% of the volume, respectively.

Figure 13b shows a further enlargement of particles of the fine fraction below  $10 \mu\text{m}$ . Again, it can be seen that the particles are of different textures—purely mineral as well as conglomerates of tire and aggregate material. The difference compared to the coarse

particles, however, is that the conglomerates contained in here do not have an elongated shape, but are rather spherical. This applies to the larger particles, as well as to the numerous small ones, which are distributed over the entire surface in this image. This fact was evident on all detailed images of the fine fraction. The assumption of spherical particles with an aspect ratio of 1 made in Section 2.2 can thus be verified.

#### 4. Discussion

When evaluating the measurement data shown in Section 3, simplifying assumptions were made which, although previously checked for plausibility, may not fully correspond to reality. For better transparency, these simplifications are explained and discussed below. In particular, the emission factors shown are scrutinized and compared with reference values from the literature. The same applies to the determination and the result of the particle density and composition.

##### 4.1. Assumptions for the Calculation of Emission Factors

For the calculation of emission factors, it was assumed that all particles emitted in the contact area between tire and road were reliably captured by the suction funnel and picked up by the volume flow. The funnel encloses the back of the wheel on a large angle and the velocity of the flow between the tire and the suction funnel amounts to 120 km/h based on the given extraction flow. Thus, the suction velocity is significantly higher than the velocity of the air flow in the drum resulting from its rotation. Since further no deposits were found in the test bench or the suction funnel, even after the entire test series, it can be presumed that the assumption of almost complete extraction is plausible.

Furthermore, it was assumed that the extraction flow is homogeneously mixed, thus making the extracted aerosol sample representative of the total flow. The degree of mixing of the extraction flow can be evaluated using the Reynolds number. If it is low, the flow is laminar, meaning that almost no mixing of the aerosol takes place. If, on the other hand, it is high, a turbulent flow is present and good mixing can be assumed [38]. With a Reynolds number of more than 200,000 in the suction pipe, the flow is turbulent ensuring good mixing of the aerosol extracted and indicating a representative sample.

In order to specify an emission factor for an entire vehicle, all wheels must be taken into account. However, since only one wheel at a time can be measured on the internal drum test bench, the emission factors calculated from the measured particle concentrations were multiplied by a factor of four. Thus, the emission factors given apply to a theoretical vehicle in which all four wheels are equally loaded with vertical, longitudinal, and lateral forces.

##### 4.2. Representativeness of the Calculated Emission Factors

When interpreting the EFs calculated, it must be kept in mind that these are snapshots, each of which represents a specific driving condition, comprising longitudinal and lateral force, of a vehicle whose wheels are loaded with a specific vertical load. The values do not correspond to the emission of a vehicle driving on open roads for a longer period of time while realistic driving behavior leads to changing forces. A realistic driving cycle which is broken down into its basic components, i.e., the individual driving conditions must therefore be used as a basis to determine real-world EFs. Each of these driving conditions can be assigned a specific EF according to Figure 9, which is valid for a certain distance traveled (corresponding to the current driving speed). The sum of the individual emissions corresponds to the total emission of a vehicle with just this vertical load. To obtain an average EF, the value can be divided by the total distance traveled.

Since no reference values for EFs at individual load conditions are known from the literature at the current time, the values obtained in this study can only be compared to long-term EFs. Some of these are compiled in Table 5.

The EFs presented were determined by sampling or measuring particles over an extended period of time, regardless of their origin or measurement method, so the influence of individual driving conditions cannot be identified. With regard to the order of magnitude,

no differences can be observed between outdoor sampling and indoor laboratories. Since there is no trend in the EF over the long period of time between publications, it can be assumed that the range from 2 mg/vkm to 11 mg/vkm is still valid for passenger cars.

**Table 5.** Compilation of emission factors from the literature.

Measurement Method	EF <sub>m</sub> in mg/vkm	Reference
Indoor laboratory	2.0–5.0	Williams & Cadle (1978) [39]
Outdoor sampling	5.0–7.2	Rauterberg-Wulff (1998) [40]
Indoor laboratory	9.0–11.0	Kupiainen et al. (2005) [22]
Outdoor sampling	2.2	Sjödin et al. (2010) [5]
Outdoor sampling	2.4–7.0	Panko et al. (2013) [10]

When comparing these values with those determined by the regression model in this study, it is noticeable that although the lower limit agrees, the calculated values for high longitudinal and lateral forces far exceed the values given in the literature. It must be taken into account that the high loads covered by the model are not occurring frequently in real-world driving. As described in Section 2.3, the range of adhesion utilization used by average drivers ends well below the limits shown. Due to these differences in measurement methodology, as well as in technology, the resulting deviation was expectable. To validate the data obtained, a simulation model based on the measured data and considering realistic driving cycles as described above is planned, which will enable comparability with the values given in the literature.

#### 4.3. Assumptions for the Determination of Particle Density and Composition

A particle sample from the dust collection box was used to determine the particle density. After sieving the sample to a maximum size of 40 µm, it was found that about 89% of this size fraction had diameters between 20 µm and 40 µm, and the remaining 11% were smaller than 20 µm. However, it is important to note that primarily coarse particles are separated in the dust collection box. Fine particles with lower mass and inertia are more likely to pass through the impact separator and the cartridge filters and are only separated in the HEPA filter, which means that they are not included in this consideration. The true fraction of particles below 20 µm is therefore probably higher than indicated here. Under this assumption, the density of the fine fraction would be somewhat lower. This, in turn, would result in a higher proportion of the tire material in the total particulate matter.

To calculate the composition of PM collected, it was assumed that only tread material from the tire and road material (aggregate, bitumen) contributed to the formation of particles. The added third-body was deliberately not taken into account, since it was assumed that a main portion of the sand had already been removed from the road surface prior to the actual measurements. In order to effectively exclude these third-body particles, the maximum forces were applied in both loading directions at the beginning of each run (see Section 2.4). Since no further significant drop in emission was observed afterwards, it can be assumed that the sand or the fragments formed from it had indeed largely left the test bench at this point. If, however, small portions of the third body remained on the roadway and were thus also included in the calculation, this could be a reason for the rather high density of the TRWP, as the density of the third body is higher than the one of the road material.

In TRWP collected on open roads, a variety of further components are found, mainly from other sources in road traffic or atmospheric sedimentation, and get incorporated in TRWP. However, due to the precautions taken (see Section 2.2) to shield particle inputs from the environment, these contributions were neglected entirely.

## 5. Conclusions

The main goal of this study was to precisely investigate the effects of longitudinal and lateral forces on the emission of tire-road PM and to determine the mathematical

correlation between the forces and the emission factor. A tire internal drum test bench has been used to run individual driving maneuvers while measuring the PM generated in real-time. The measured data were used to calculate EFs for individual driving conditions. It was found that the relationship between horizontal tire forces and the emission can best be approximated by fourth-order regression functions. Furthermore, it became apparent that for the summer tire investigated, lateral forces lead to an emission that is about four times higher than the emission caused by equivalent longitudinal forces—a trend that was also confirmed for other summer tire models. Thus, emission factors of about 89 mg/vkm and 335 mg/vkm in the longitudinal and lateral direction, respectively, resulted for the maximum force applied. These extremely high values represent snapshots which hardly occur in real-world driving, since they involve maneuvers in the driving dynamic threshold range.

From the individual emission functions determined for longitudinal, lateral, and combined tire forces, a three-dimensional function was determined analytically that provides the EF for any horizontal tire–road forces. In order to derive an EF for an average drive on open roads, it is planned to use a real driving cycle, to assign an emission to each driving condition contained and to sum add up the individual emissions. In its current state, the function used is only valid for one vertical load and will be extended by further tests to take into account the influence of vertical load.

In addition to the pure amount of emission, the particle size distribution was recorded throughout the tests. Regardless of the load condition (horizontal forces), the data reveals bimodal distributions with one peak at about 1.8  $\mu\text{m}$  and one most likely below the lower detection limit of the aerosol spectrometer (0.3  $\mu\text{m}$ ). Furthermore, it was found that the particle size distribution changes depending on the load condition. A high horizontal force leads to increased emission of larger particles. This means that the particle emission increases with increasing force over the entire particle size range ( $0.3 \mu\text{m} < d_p < 10 \mu\text{m}$ ), but the largest rises occur for large particles ( $6 \mu\text{m} < d_p < 10 \mu\text{m}$ ).

Finally, the particles collected were separated into size fractions and subjected to density measurements to derive conclusions regarding their composition. The finest fraction obtained ( $d_p < 20 \mu\text{m}$ ) had a density of 2.299 g/cm<sup>3</sup>, and consisted of 18% by weight tire material. The remaining 82% derived from the aggregate and the bitumen of the road. Transferred to the volume, the proportions are 32% and 68%, respectively. Scanning Electron Microscope (SEM) images of the collected particles confirm the plausibility of the values calculated. The images show that the shape of TRWP ( $d_p < 20 \mu\text{m}$ ) emitted as PM seems to be spherical, which deviates from the elongated shape found for coarse particles and also reported in the literature [37]. However, this statement generally refers to coarser TRWP ( $d_p > 20 \mu\text{m}$ ), so the result found here is not contradictory.

The results show the major influence of driving behavior on the emission of tire–road PM. This is accompanied by the importance of an anticipatory and restrained driving style for minimizing emissions.

**Author Contributions:** Conceptualization, S.S., H.-J.U.; methodology, S.S.; software, S.S.; validation, S.S., H.-J.U.; formal analysis, S.S.; investigation, S.S.; resources, F.G.; data curation, S.S.; writing—original draft preparation, S.S.; writing—review and editing, H.-J.U.; visualization, S.S.; supervision, S.S.; project administration, S.S.; funding acquisition, F.G. All authors have read and agreed to the published version of the manuscript.

**Funding:** This research is funded by the KIT-Publication Fund of the Karlsruhe Institute of Technology.

**Institutional Review Board Statement:** Not applicable.

**Informed Consent Statement:** Not applicable.

**Data Availability Statement:** Restrictions apply to the availability of these data. Due to a non-disclosure agreement, the data are only available from the corresponding author with the permission of the Mercedes-Benz Group AG.

**Acknowledgments:** We would like to thank Mercedes-Benz Group AG, which made a significant contribution to this study by funding the framework project “Influence of driving conditions on particulate emissions from tires and roads”. Furthermore, we would like to thank the Institute of Highway and Railroad Engineering (ISE) of KIT for the possibility to sieve the particle fractions and the Institute for Applied Materials (IAM-ESS) for performing the density measurements.

**Conflicts of Interest:** The authors declare that they have no known competing financial interests or personal relationships that could have appeared to influence the work reported in this paper.

## Abbreviations

The following abbreviations are used in this manuscript:

EF	Emission Factor
FAST	Institute of Vehicle System Technology
KIT	Karlsruhe Institute of Technology
PM	Particulate Matter
PMC	Particle Mass Concentration
PNC	Particle Number Concentration
SEM	Scanning Electron Microscope
SRT	Skid Resistance Tester
TRWP	Tire and Road Wear Particles

## References

- European Commission. *Regulation of the European Parliament and of the Council: On Type-Approval of Motor Vehicles and Engines and of Systems, Components and Separate Technical Units Intended for Such Vehicles, with Respect to Their Emissions and Battery Durability (Euro 7) and Repealing Regulations (EC) No 715/2007 and (EC) No 595/2009*; European Commission: Brussels, Belgium, 2022.
- Timmers, V.R.J.H.; Achter, P.A.J. Non-exhaust PM emissions from electric vehicles. *Atmos. Environ.* **2016**, *134*, 10–17. [[CrossRef](#)]
- Luhana, L.; Sokhi, R.; Warner, L.; Mao, H.; Boulter, P.; McCrae, I.; Wright, J.; Osborn, D. *Measurement of Non-Exhaust Particulate Matter: PARTICULATES—Characterisation of Exhaust Particulate Emissions from Road Vehicles*; European Commission: Brussels, Belgium, 2004.
- Bukowiecki, N.; Lienemann, P.; Hill, M.; Furger, M.; Richard, A.; Amato, F.; Prévôt, A.; Baltensperger, U.; Buchmann, B.; Gehrig, R. PM10 emission factors for non-exhaust particles generated by road traffic in an urban street canyon and along a freeway in Switzerland. *Atmos. Environ.* **2010**, *44*, 2330–2340. [[CrossRef](#)]
- Sjödin, Å.; Ferm, M.; Björk, A.; Rahmberg, M.; Gudmundsson, A.; Swietlicki, E.; Johansson, C.; Gustafsson, M.; Blomqvist, G. *Wear Particles from Road Traffic: A Field, Laboratory and Modelling Study: Final Report*; IVL Swedish Environmental Research Institute Ltd.: Göteborg, Sweden, 2010.
- Amato, F.; Schaap, M.; van der Denier Gon, H.A.; Pandolfi, M.; Alastuey, A.; Keuken, M.; Querol, X. Effect of rain events on the mobility of road dust load in two Dutch and Spanish roads. *Atmos. Environ.* **2012**, *62*, 352–358. [[CrossRef](#)]
- Harrison, R.M.; Jones, A.M.; Gietl, J.; Yin, J.; Green, D.C. Estimation of the contributions of brake dust, tire wear, and resuspension to nonexhaust traffic particles derived from atmospheric measurements. *Environ. Sci. Technol.* **2012**, *46*, 6523–6529. [[CrossRef](#)] [[PubMed](#)]
- Kam, W.; Liacos, J.W.; Schauer, J.J.; Delfino, R.J.; Sioutas, C. Size-segregated composition of particulate matter (PM) in major roadways and surface streets. *Atmos. Environ.* **2012**, *55*, 90–97. [[CrossRef](#)]
- Amato, F.; Pandolfi, M.; Alastuey, A.; Lozano, A.; Contreras González, J.; Querol, X. Impact of traffic intensity and pavement aggregate size on road dust particles loading. *Atmos. Environ.* **2013**, *77*, 711–717. [[CrossRef](#)]
- Panko, J.M.; Chu, J.; Kreider, M.L.; Unice, K.M. Measurement of airborne concentrations of tire and road wear particles in urban and rural areas of France, Japan, and the United States. *Atmos. Environ.* **2013**, *72*, 192–199. [[CrossRef](#)]
- Lawrence, S.; Sokhi, R.; Ravindra, K. Quantification of vehicle fleet PM10 particulate matter emission factors from exhaust and non-exhaust sources using tunnel measurement techniques. *Environ. Pollut.* **2016**, *210*, 419–428. [[CrossRef](#)]
- Etyemezian, V.; Kuhns, H.; Gillies, J.; Chow, J.; Hendrickson, K.; McGown, M.; Pitchford, M. Vehicle-based road dust emission measurement (III): Effect of speed, traffic volume, location, and season on PM10 road dust emissions in the Treasure Valley, ID. *Atmos. Environ.* **2003**, *37*, 4583–4593. [[CrossRef](#)]
- Hussein, T.; Johansson, C.; Karlsson, H.; Hansson, H.C. Factors affecting non-tailpipe aerosol particle emissions from paved roads: On-road measurements in Stockholm, Sweden. *Atmos. Environ.* **2008**, *42*, 688–702. [[CrossRef](#)]
- Mathissen, M.; Scheer, V.; Vogt, R.; Benter, T. Investigation on the potential generation of ultrafine particles from the tire–road interface. *Atmos. Environ.* **2011**, *45*, 6172–6179. [[CrossRef](#)]
- Kupiainen, K.J.; Pirjola, L. Vehicle non-exhaust emissions from the tyre–road interface—Effect of stud properties, traction sanding and resuspension. *Atmos. Environ.* **2011**, *45*, 4141–4146. [[CrossRef](#)]

16. Mathissen, M.; Scheer, V.; Kirchner, U.; Vogt, R.; Benter, T. Non-exhaust PM emission measurements of a light duty vehicle with a mobile trailer. *Atmos. Environ.* **2012**, *59*, 232–242. [[CrossRef](#)]
17. Kwak, J.; Lee, S.; Lee, S. On-road and laboratory investigations on non-exhaust ultrafine particles from the interaction between the tire and road pavement under braking conditions. *Atmos. Environ.* **2014**, *97*, 195–205. [[CrossRef](#)]
18. Aatmeeeyata; Kaul, D.S.; Sharma, M. Traffic generated non-exhaust particulate emissions from concrete pavement: A mass and particle size study for two-wheelers and small cars. *Atmos. Environ.* **2009**, *43*, 5691–5697. [[CrossRef](#)]
19. Kim, G.; Lee, S. Characteristics of Tire Wear Particles Generated by a Tire Simulator under Various Driving Conditions. *Environ. Sci. Technol.* **2018**, *52*, 12153–12161. [[CrossRef](#)]
20. Park, I.; Kim, H.; Lee, S. Characteristics of tire wear particles generated in a laboratory simulation of tire/road contact conditions. *J. Aerosol Sci.* **2018**, *124*, 30–40. [[CrossRef](#)]
21. Foitzik, M.J.; Unrau, H.J.; Gauterin, F.; Dornhöfer, J.; Koch, T. Investigation of Ultra Fine Particulate Matter Emission of Rubber Tires. *Wear* **2018**, *394–395*, 87–95. [[CrossRef](#)]
22. Kupiainen, K.J.; Tervahattu, H.; Räisänen, M.; Mäkelä, T.; Aurela, M.; Hillamo, R. Size and composition of airborne particles from pavement wear, tires, and traction sanding. *Environ. Sci. Technol.* **2005**, *39*, 699–706. [[CrossRef](#)]
23. Dahl, A.; Gharibi, A.; Swietlicki, E.; Gudmundsson, A.; Bohgard, M.; Ljungman, A.; Blomqvist, G.; Gustafsson, M. Traffic-generated emissions of ultrafine particles from pavement-tire interface. *Atmos. Environ.* **2006**, *40*, 1314–1323. [[CrossRef](#)]
24. Gustafsson, M.; Blomqvist, G.; Gudmundsson, A.; Dahl, A.; Swietlicki, E.; Bohgard, M.; Lindbom, J.; Ljungman, A. Properties and toxicological effects of particles from the interaction between tyres, road pavement and winter traction material. *Sci. Total. Environ.* **2008**, *393*, 226–240. [[CrossRef](#)] [[PubMed](#)]
25. Gustafsson, M.; Blomqvist, G.; Gudmundsson, A.; Dahl, A.; Jonsson, P.; Swietlicki, E. Factors influencing PM10 emissions from road pavement wear. *Atmos. Environ.* **2009**, *43*, 4699–4702. [[CrossRef](#)]
26. Panko, J.; McAtee, B.L.; Kreider, M.; Gustafsson, M.; Blomqvist, G.; Gudmundsson, A.; Sweet, L.; Finley, B. Physio-Chemical Analysis of Airborne Tire Wear Particles. In Proceedings of the 46th Congress of the European Societies of Toxicology, Dresden, Germany, 13–16 September 2009.
27. Schläfle, S.; Gauterin, F.; Lallement, R. Aufbau eines Prüfstands zur Messung von Reifen-Fahrbahn-Feinstaubemissionen auf realen Fahrbahnoberflächen. In *Proceedings of the Reifen—Fahrwerk—Fahrbahn*; VDI Wissensforum GmbH, Ed.; VDI Verlag: Düsseldorf, Germany, 2022; VDI-Berichte 2398, pp. 15–33. [[CrossRef](#)]
28. Schläfle, S.; Unrau, H.J.; Gauterin, F. Influence of Load Condition, Tire Type, and Ambient Temperature on the Emission of Tire–Road Particulate Matter. *Atmosphere* **2023**, *14*, 1095. [[CrossRef](#)]
29. ISO 9096:2017; Stationary Source Emissions—Manual Determination of Mass Concentration of Particulate Matter. International Organization for Standardization: Geneva, Switzerland, 2017.
30. PALAS. Datasheet Promo 2000. Available online: <https://www.palas.de/en/product/download/promo2000/datasheet/pdf> (accessed on 13 June 2022).
31. PALAS. Datasheet Aerosol Sensor Welas 2500. Available online: [https://www.palas.de/en/product/download/aerosolsensor\\_welas2500/datasheet/pdf](https://www.palas.de/en/product/download/aerosolsensor_welas2500/datasheet/pdf) (accessed on 13 June 2022).
32. EN 13036; Road and Airfield Surface Characteristics—Test Methods—Part 4: Method for Measurement of Slip/Skid Resistance of a Surface—The Pendulum Test. European Committee for Standardization: Berlin, Germany, 2011.
33. Jansen, D.; Pöppel-Decker, M. *Griffigkeitsprognose an Offenporigen Asphalten—Teil 2: Neue Baumaßnahmen*; Heft S 72, Bundesanstalt für Straßenwesen, Wirtschaftsverl. für neue Wiss: Bergisch Gladbach, Germany, 2011.
34. Forschungsgesellschaft für Straßen- und Verkehrswesen. *Zusätzliche technische Vertragsbedingungen und Richtlinien für den Bau von Verkehrsflächenbefestigungen aus Asphalt: ZTV Asphalt-StB 07*; FGGSV: Cologne, Germany, 2013.
35. Kayhanian, M.; McKenzie, E.R.; Leatherbarrow, J.E.; Young, T.M. Characteristics of road sediment fractionated particles captured from paved surfaces, surface run-off and detention basins. *Sci. Total. Environ.* **2012**, *439*, 172–186. [[CrossRef](#)]
36. Kovochich, M.; Liong, M.; Parker, J.A.; Oh, S.C.; Lee, J.P.; Xi, L.; Kreider, M.L.; Unice, K.M. Chemical mapping of tire and road wear particles for single particle analysis. *Sci. Total. Environ.* **2021**, *757*, 144085. [[CrossRef](#)]
37. Baensch-Baltruschat, B.; Kocher, B.; Stock, F.; Reifferscheid, G. Tyre and road wear particles (TRWP)—A review of generation, properties, emissions, human health risk, ecotoxicity, and fate in the environment. *Sci. Total. Environ.* **2020**, *733*, 137823. [[CrossRef](#)]
38. Hinds, W.C. *Aerosol Technology: Properties, Behavior, and Measurement of Airborne Particles*, 2nd ed.; Wiley-Interscience: New York, NY, USA, 1999.
39. Williams, R.L.; Cadle, S.H. Characterization of Tire Emissions Using an Indoor Test Facility. *Rubber Chem. Technol.* **1978**, *51*, 7–25. [[CrossRef](#)]
40. Rauterberg-Wulff, A. *Beitrag des Reifen- und Bremsenabriebs zur Rußemission an Straßen*; Fortschritt-Berichte VDI: Reihe 15, Umwelttechnik; VDI-Verlag: Düsseldorf, Germany, 1998.

**Disclaimer/Publisher’s Note:** The statements, opinions and data contained in all publications are solely those of the individual author(s) and contributor(s) and not of MDPI and/or the editor(s). MDPI and/or the editor(s) disclaim responsibility for any injury to people or property resulting from any ideas, methods, instructions or products referred to in the content.